Estimating climatically relevant singular vectors for decadal predictions of the Atlantic Ocean

Ed Hawkins* and Rowan Sutton
NCAS-Climate, Department of Meteorology, University of Reading

Accepted by J. Climate

* *Corresponding author address:* Ed Hawkins, Department of Meteorology, University of Reading, Reading. RG6 6BB. UK. E-mail: e.hawkins@reading.ac.uk

ABSTRACT

A key aspect in designing an efficient decadal prediction system is ensuring that the uncertainty in the ocean initial conditions is sampled optimally. Here, we consider one strategy to address this issue by investigating the growth of optimal perturbations in the HadCM3 global climate model (GCM). More specifically, climatically relevant singular vectors (CSVs) - the small perturbations which grow most rapidly for a specific initial condition - are estimated for decadal timescales in the Atlantic Ocean. It is found that reliable CSVs can be estimated by running a large ensemble of integrations of the GCM. Amplification of the optimal perturbations occurs for more than 10 years, and possibly up to 40 years. The identified regions for growing perturbations are found to be in the far North Atlantic, and these perturbations cause amplification through an anomalous meridional overturning circulation response. Additionally, this type of analysis potentially informs the design of future ocean observing systems by identifying the sensitive regions where small uncertainties in the ocean state can grow maximally. Although these CSVs are expensive to compute, we identify ways in which the process could be made more efficient in the future.

1. Introduction

Successful predictions of changes in climate for the forthcoming decade, especially on regional and local scales, depend on predicting both the continuing response of the climate to radiative forcings, and the natural decadal climate variations which mainly arise from slow changes in the oceans (e.g. Hawkins and Sutton 2009b). Most current climate projections, including the IPCC AR4 (Meehl et al. 2007), only consider the changes in radiative forcings. The potential for enhanced skill has led to the design of decadal climate prediction systems which initialise climate forecasts from the observed ocean state (e.g. Smith et al. 2007; Keenlyside et al. 2008; Pohlmann et al. 2009). Initialised forecasts also offer a new way of testing and validating climate models, and a multi-model intercomparison is planned for the next IPCC report (Meehl et al. 2009).

The Atlantic Ocean is of particular importance because of its central role in the global overturning circulation. There is evidence from global climate models (GCMs) that variations in the Atlantic meridional overturning circulation (MOC) are largely responsible for the observed decadal changes in Atlantic sea surface temperatures (SSTs) and hence can influence the atmosphere, and that these variations are potentially predictable on decadal timescales (e.g. Griffies and Bryan 1997; Pohlmann et al. 2004; Collins et al. 2006; Hawkins et al. 2010).

One key challenge is to improve our understanding of error growth on decadal timescales, and this is important for several reasons. Firstly, understanding why, and how quickly, a climate model, initialised from the observations, diverges from subsequent observations is valuable for identifying the specific physical processes responsible for error growth. Improving the representation of these key processes in GCMs might then become a priority.

Secondly, identifying the ocean regions which are most sensitive to small perturbations will therefore also allow the design of optimal observing systems to constrain predictions in a targeted, cost-effective way. This improvement is especially important for the oceans because of the high cost of sub-surface observations. Thirdly, understanding perturbation growth is required to design efficient ensembles to sample initial condition uncertainty (e.g. Molteni et al. 1996). For example, in the UK Met Office's Decadal Prediction System (DePreSys; Smith et al. 2007), which is based on the HadCM3 GCM, an ensemble of forecasts is currently generated by using essentially identical ocean states, but with different atmospheric states, in the initial conditions. This causes the forecasts to diverge, even in the ocean, giving a spread, or uncertainty, in the prediction. However, there is evidence that the spread of these ensemble members is too narrow when compared with the observations, i.e. the estimated uncertainties in the forecasts are not reliable (Smith et al. 2007). There is therefore a need to design initial condition perturbations which will ensure a reliable spread.

Optimal perturbations, these being the perturbations that grow most rapidly over a defined time interval (e.g. Farrell 1988), are routinely used in numerical weather prediction (NWP) to ensure reliable ensemble spreads and to identify regions for targeted observations (e.g. Palmer et al. 1998). Several techniques exist for generating such optimal perturbations, such as singular vectors (e.g. Buizza and Palmer 1995) or breeding vectors (e.g. Toth and Kalnay 1997). However, in NWP it is the rapidly growing weather modes that are important, but on longer (seasonal to decadal) timescales it is necessary to remove any effect of rapidly growing weather perturbations and instead focus on the fastest growing climate perturbations.

Several methods exist for estimating optimal perturbations for climate timescales. Singular vectors have been estimated in simplified climate models (e.g. Zanna and Tziperman 2005; Sevellec et al. 2007; Zanna et al. 2010) and both Sevellec et al. (2008) and Czeschel et al. (2010) examined the sensitivity of the MOC to perturbations and surface forcings using adjoints of ocean-only models. However, it is important to consider the role of coupled processes. To our knowledge, no explicit adjoint has yet been developed for a full coupled GCM and there is therefore a need to consider approximate methods. Other studies (e.g. Tziperman et al. 2008; Hawkins and Sutton 2009a) have estimated optimal perturbations for decadal predictions of the Atlantic Ocean in GCMs using linear inverse modelling [LIM; see e.g. Penland and Sardeshmukh (1995) for more details] instead. This statistical methodology allows the calculation of an optimal perturbation averaged over many different initial conditions, and thus removes the 'weather noise'. Both Tziperman et al. (2008) and Hawkins and Sutton (2009a) (hereafter HS09) found that the far North Atlantic was the optimal initial perturbation region in the GCMs considered. In the HadCM3 GCM, growth occurred for more than 30 years through an initial induced change in the meridional overturning circulation (MOC), followed by a slower spreading of anomalies southwards and into the deeper ocean (HS09). Tziperman et al. (2008) found a similar mechanism in the GFDL CM2.1 GCM, but the growth occurred over shorter lead times.

However, it is important to note that the growth of perturbations not only depends on

the structure of the perturbation and the norm used to measure growth, but also on the ocean state at the time the perturbation occurs, i.e. the growth of perturbations is initial state dependent, even in very simple systems (e.g. Palmer 1993). Kleeman et al. (2003) (hereafter KTM03) describe a methodology to estimate climatically relevant singular vectors (CSVs) from a GCM for specific initial states by running a large ensemble of integrations to average out the weather noise. They applied their methodology to estimate CSVs for seasonal forecasting of SST in the Pacific Ocean, and found that their leading CSV grew into a structure resembling the mature phase of an El Niño-Southern Oscillation event. However, for decadal climate predictions, it is likely that perturbations over the entire ocean depth, and to salinity as well as temperature, will result in the largest growth.

Our study investigates the growth, on decadal timescales, of perturbations in the Atlantic Ocean. More specifically, we aim to estimate optimal perturbations in a GCM for specific initial conditions with the motivation of using the perturbations in decadal predictions of the Atlantic Ocean. We therefore extend and adapt the methodology of KTM03 to allow the estimation of CSVs for decadal, rather than seasonal, timescales. To do this requires including information from the surface and deeper ocean, and to consider the effects of both temperature and salinity, and hence density. We use the HadCM3 GCM to allow a direct comparison with the more statistical LIM approach (HS09).

This paper is structured as follows. Section 2 describes the model and methodology used, and Section 3 examines the properties of the leading CSV. In Section 4 we confirm that the estimated CSV works as predicted, and examine the mechanism of amplification. We conclude and discuss the results in Section 5.

2. Model description and methodology

a. Details of HadCM3

In the subsequent analysis we use the third UK Hadley Centre global, coupled ocean-atmosphere model (HadCM3). Gordon et al. (2000) describe HadCM3 in detail, and here we give a brief summary. HadCM3 has an atmospheric resolution of $2.5° \times 3.75°$ and 19 vertical levels coupled to an ocean component which has a resolution of $1.25° \times 1.25°$ with 20 vertical levels. The model does not require flux adjustment to maintain a stable climate. The mean state of the ocean model matches observed values to within 1 K and 1 psu in most regions (Gordon et al. 2000; Pardaens et al. 2003). The relatively coarse resolution of the model allows for the several millennia of integrations required in our analysis (see below) to be run in a reasonable time. Smith et al. (2007) describe the use of this GCM for decadal climate predictions and demonstrate enhanced skill of initialised retrospective forecasts from 1981-2001, as compared to uninitialised projections with the same model.

b. Estimation of climatic singular vectors

A general dynamical system can be written as,

$$\phi(t + \Delta t) = F[\phi(t)], \tag{1}$$

where ϕ is the state vector of the system and F represents a complicated, non-linear, operator. For 'small' perturbations ($\delta\phi$), the evolution of the system can be approximated by,

$$\delta\phi(t + \Delta t) = \mathbf{R}\delta\phi(t), \tag{2}$$

where $\mathbf{R}$ is a linear operator. The singular vectors of the system, which are the perturbations which amplify maximally over time Δt, are the eigenvectors of $\mathbf{R}^{\mathrm{T}}\mathbf{R}$ with the largest real part (e.g. Buizza and Palmer 1995), where $\mathbf{R}^{\mathrm{T}}$ is the transpose of $\mathbf{R}$.

For an atmosphere-ocean coupled GCM this conceptually simple framework becomes more complicated as $\mathbf{R}$ is not directly available. Firstly, the state vector of the system is enormous, requiring the system to be represented in a reduced state space. This reduction is often achieved by isolating the leading modes of variability, e.g. by using empirical orthogonal functions (EOFs) [see Farrell and Ioannou (2001), Moore and Kleeman (2001) and KTM03 for extensive discussions]. Secondly, when considering climatic timescales the presence of weather 'noise' requires a modified strategy because different realisations of the weather may cause different climate outcomes. To address this issue it is necessary to average over many realisations of the weather to obtain a climatically relevant singular vector. Thus, a propagator $\mathbf{R}$ can be estimated (Gardiner 1985; KTM03) using,

$$\overline{\delta\psi(t_0 + \Delta t)} = \mathbf{R}\delta\psi(t_0), \tag{3}$$

where ψ is the reduced state vector of the system and $\overline{\delta\psi}$ represents an ensemble mean. The different ensemble members are constructed with tiny perturbations to $\psi(t_0)$ which cause the weather to diverge.

c. Application to decadal timescales in HadCM3

KTM03 used the above methodology to estimate singular vectors for SST on seasonal timescales in the Pacific Ocean. We extend the methodology to estimate climatic singular vectors for decadal timescales in the Atlantic basin. Amplification on decadal timescales will likely involve the deeper ocean due to the dynamics of the meridional overturning circulation, and hence the density structure. It is therefore necessary to consider three spatial dimensions, and both salinity and temperature, rather than just SST.

The details of this process are now described. In all that follows we use annual mean fields, except for the instantaneous initial conditions.

i. Calculate the leading 3d joint, correlation[1] EOFs (denoted E_i) of ocean temperature and salinity from a long (1600 year) pre-industrial control integration of HadCM3

[1]Moore and Kleeman (2001) discuss why it is important to use correlation EOFs to retain regions with small absolute variability, but from where anomalies can still grow rapidly, e.g. the deep ocean.

in the chosen domain (20°S-90°N, 100°W-20°E, from the surface to 1800m depth)[2]. Hawkins and Sutton (2007) (hereafter HS07) describe the estimation and properties of these EOFs in more detail, but it is important to note that the temperature and salinity fields are weighted by their contribution to local density anomalies.

ii. Choose a suitable initial condition from the control integration; we chose 1st December, after 1050 years of the control run. This choice was made partly because of the availability of model initial conditions and partly because the model state in the Atlantic was not particularly unusual at that time (in the subspace of the leading two EOFs - see HS07). The instantaneous ocean temperature and salinity anomalies from the time mean are shown in Fig. 1a, and the meridional overturning index (MOI) around the start date is shown in Fig. 1b.

iii. Run a control ensemble (with K members) from the chosen initial condition for T years. The ensemble mean of the ocean temperature and salinity fields over the chosen domain, is denoted by $\overline{\psi_0}(t)$. The different ensemble members are generated by perturbing the SST field globally by different realisations of random Gaussian white noise with variance 10^{-8}K. These small perturbations cause the atmospheric states to diverge rapidly.

iv. Run M separate ensembles (each with K members) for T years from the chosen initial condition, with the i-th ensemble perturbed in salinity and temperature by the i-th EOF (E_i), so

$$\delta\psi_i(t_0) = E_i. \tag{4}$$

We scale the EOFs by a factor of 0.4 to try to remain in the linear regime. The spatial domain of the EOFs is extended to all depths and into the Arctic by regressing the appropriate principal components (PCs) against salinity and temperature in these regions. Furthermore, the anomalies are tapered to zero at the southern boundary (20°S) to minimise any sudden unwanted ocean readjustment. The different members of each ensemble are generated as for the control ensemble. The ensemble means of ocean temperature and salinity are denoted by $\overline{\psi_i}(t)$, where $1 \leq i \leq M$.

v. The difference between the mean of ensemble i and the mean of the control ensemble is,

$$P_i(t) = \overline{\psi_i(t)} - \overline{\psi_0(t)} = \overline{\delta\psi_i(t)}, \tag{5}$$

where t represents $t_0 + \Delta t$, following Eqn. 3. An approximate (tangent linear) propagator matrix ($\mathbf{R}$) is assumed to model the evolution of the ensemble mean anomalies in the subspace of the leading M EOFs. So, from Eqn. 3,

$$\mathbf{R}(\mathbf{W} \bullet \mathbf{E}) = (\mathbf{W} \bullet \mathbf{P}) + \text{residuals}, \tag{6}$$

[2]We note that potential global teleconnections from the Antarctic Circumpolar Current or Agulhas region may be missed by restricting the EOFs to northwards of 20°S, but this was done because of computational constraints.

where the rows of $\mathbf{E}$ are the EOFs (E_i), the rows of $\mathbf{P}$ are P_i, $\mathbf{W}$ is a matrix of weights and $\bullet$ represents the matrix entry-wise product. In the estimation of the EOFs various weightings are used for latitude, depth, local standard deviation and contribution to local density (see HS07); $\mathbf{W}$ is a combination of all these factors and is required to ensure the deep ocean is represented and that each volume of water is treated equally.

vi. Eqn. 6 is solved approximately for $\mathbf{R}$ by minimising the residual term. As $\mathbf{P}$ is lead time dependent, the propagator $\mathbf{R}$ can be estimated for different lead times.

vii. The CSVs ($\mathbf{x}$) are then the solutions of,

$$\mathbf{R}^{\mathrm{T}}\mathbf{N}\mathbf{R}\mathbf{x} = \lambda^2\mathbf{N}\mathbf{x} \tag{7}$$

where $\mathbf{N}$ is the norm under which the amplification (λ^2) is maximised. The CSVs, $\mathbf{x}$, can then transformed back into real space ($\mathbf{x}^{\mathrm{T}}\mathbf{E}$). In this analysis, a quadratic norm is used ($\mathbf{N} = \mathbf{I}$, the identity matrix), although Section 3.c briefly explores the sensitivity to this choice.

viii. To demonstrate that the CSV amplifies as predicted by the linear propagator, the amplified singular vector in real space, $(\mathbf{R}\mathbf{x})^{\mathrm{T}}\mathbf{E}$, can be compared to the pattern that is derived from running an additional ensemble of the full GCM with the same initial condition perturbed with the CSV.

ix. The steps ii-viii can be repeated for a different initial condition from the control integration.

This methodology has the advantage that the choice of norm and optimisation lead time can be made after the ensembles have been completed - they do not have to be chosen beforehand. The sensitivity to these choices can therefore be explored without further model integrations. However, we note that this process estimates the optimally growing mode in the sub-space of the leading EOFs of the ocean variability. It is possible that a more optimally amplifying mode exists which we cannot capture with this approximation.

d. Choice of parameters

This method thus requires an 'ensemble of ensembles', with a total of $K \times (M+1)$ members, each run for T years, per initial condition. This is potentially an extremely expensive computational task. Previous results with HadCM3 (HS09) indicate that amplification can occur for more than 30 years in the Atlantic. Each ensemble was therefore chosen to be run for $T = 40$ years, with $K = 16$ members, to ensure a reliable estimate of the mean response. Computational resources allowed us to run $M = 8$ ensembles for a single initial condition[3]; these leading 8 EOFs account for 46% of the total 3d variance in temperature and salinity. The sensitivity to these choices is explored below.

[3]This choice of parameters amounts to nearly 6000 years of model integration, using around 20 CPU-years.

An operational decadal prediction system would likely only consider singular vectors for, at most, 10 year lead times, and hence the computational cost could be reduced by at least a factor of four in this case. As shown below this reduced lead time for optimisation may also allow smaller ensembles to be run, reducing the computational expense further.

3. The climatic singular vectors

a. The leading CSV

The leading CSVs and singular values (λ) are estimated for lead times up to 40 years following the above methodology.

We first consider the leading singular vector, optimised for maximum growth at a lead time of 10 years, which shows an amplification of $\lambda \approx 2$ (see below); this is an example of a perturbation that could be used in an operational decadal prediction system. The optimal initial pattern for temperature, salinity and density is shown in Fig. 2. Note that the surface perturbation, in both temperature and salinity, has large values in the North Atlantic Current (NAC) region, and in the Nordic and Labrador Seas, which is where deep convection occurs in this GCM (Grist et al. 2007). At deeper levels, the NAC and northern coast of South America regions dominate. Note also that the temperature and salinity fields are substantially density compensating, but temperature tends to dominate. The optimal perturbation has a north-south density gradient in the far north Atlantic, which is likely to cause an MOC acceleration in this GCM (Thorpe et al. 2001; Dong and Sutton 2005).

The amplified pattern, after 10 years, is shown in Fig. 3. The main development is a strengthening of the North Atlantic Current warm and salty anomaly, and there is some propagation of anomalies southwards along the western boundary at depth (similarly to HS09).

b. Robustness of CSVs

Before examining the amplification in more detail, it is first necessary to establish that the CSVs are robust to the various choices made in the methodology, especially the number of EOFs retained (M) and the number of ensemble members used (K).

1) Number of EOFs required

The leading singular values (λ as a function of lead time), using different numbers of EOFs in their estimation, are shown in Fig. 4, for a fixed $K = 16$. Significant amplification is seen, even with a relatively small number of EOFs, and the amplification seems to be converging for 8 EOFs (solid orange line). The shapes of the curves when using different numbers of EOFs are quite consistent, suggesting that the dominant features of the amplification are captured in the leading EOF modes. The double peak structure suggests that there may be two timescales and mechanisms of amplification, or that we do not have enough

ensemble members to adequately describe the growth for lead times longer than ~ 15 years (see below)[4].

It is also necessary to ensure that the initial CSV patterns themselves are converging. Fig. 5 shows the leading CSV pattern for temperature, using different numbers of EOFs, optimised for maximum amplification after 33 years. Again, convergence of the optimally growing pattern can be seen, with increasing resolution of small scale features, especially in the North Atlantic Current region. A similar convergence is seen for the salinity field (not shown). The structure of the final amplified state also converges (not shown), although the amplitude of the anomalies increases, consistent with Fig. 4.

2) Number of ensemble members required

Fig. 6 shows how the maximal amplification changes for differing numbers of ensemble members (K), when using $M = 8$ EOFs. If just 4 ensemble members are used then a large maximal amplification is seen ($\lambda > 10$, dashed grey line). The maximal amplification is smaller when using more ensemble members as the true ocean mean is being captured more effectively. For lead times larger than about 15 years, the amplification does not appear to have converged even when using 16 members, and so this amplification estimate must be viewed as an upper bound. It can be seen that 8-12 members might be enough for exploring amplification for lead times of 10 years or less, which would further reduce the computational cost of this type of analysis in an operational decadal prediction system.

KTM03 also found that the singular value converged relatively slowly when adding additional ensemble members, but that the CSV initial pattern converged more quickly. Fig. 7 shows how the initial CSV pattern for temperature converges with the number of members used in each ensemble, always using 8 EOFs and for a lead time of 33 years. The similarity of the spatial patterns when using 12 and 16 members suggests that the pattern has converged. A similar convergence is seen for the salinity field (not shown). The structure of the final amplified state also converges (not shown), although the amplitude of the anomalies decreases, consistent with Fig. 6.

c. Sensitivity to choice of norm

Although the amplification is explored below for the optimal perturbations already described using the identity matrix as the norm, $\mathbf{N}=\mathbf{I}$, we briefly explore the sensitivity of the CSVs to this choice. Following HS09, we consider, firstly, a norm which specifically finds the optimal perturbations which cause growth in anomalies of the MOC (denoted by $\mathbf{N}_{\mathrm{MOC}}$ in HS09) and, secondly, a norm which maximises the changes in total variance (denoted by $\mathbf{N}_{\mathrm{V}}$ in HS09). In both cases, the optimal initial perturbations and patterns of growth over the first decade are almost identical to using the identity matrix as the norm (not shown),

[4]Alternative explanations could include growth temporarily occurring in covariances of temperature and salinity, causing the apparent amplification to decrease, or even that there is growth in density anomalies through cancellation of temperature and salinity anomalies.

giving us confidence that our growth is robust.

However, specific norms which explore growth in just SSTs, or in certain regions of the Atlantic, would produce different results, but this is beyond the scope of this paper.

4. Do the estimated CSVs work?

The CSVs described above are estimated from a linear approximation to the non-linear GCM. Therefore, the next step in the analysis is to examine whether the calculated CSVs actually produce similar growth when added to the same initial conditions and run forwards in HadCM3. Note also that the sign of the perturbation is arbitrary as we have assumed linearity, and so we consider both positive and negative projections of the leading CSV.

a. Scaling the CSV

A key question when using the estimated CSV is choosing the amplitude of the initial condition perturbation. An operational decadal climate forecast system will use an ocean analysis as the initial condition, but this ocean state will be uncertain. For the CSV to be of optimal use in such a system, the amplitude of the perturbation pattern should be close to the uncertainty in the ocean analysis. Thus the estimated CSV needs to be scaled to an appropriate amplitude.

Although it is not easy to estimate a scaling rigorously, an estimate can be obtained (Greg Smith, personal communication) from the spread between different estimates of ocean analyses produced by different research groups, e.g. the CLIVAR Global Synthesis and Observations Panel (GSOP). This method gives an estimate of approximately 0.4× the estimated CSV pattern, which results in a perturbation amplitude corresponding to 10-20% of the interannual variability. In operational NWP, the amplitudes of perturbations are broadly similar in terms of % of daily variability (Toth and Kalnay 1997).

b. Level of amplification

To ensure a large response, we choose to consider the largest amplifying CSV, i.e. that which amplifies maximally after 33 years and run two further ensembles from the same initial state, perturbed with the positive and negative projections of the CSV pattern, scaled by 0.4. Fig. 8 shows that the amplification of the positive projection of the leading CSV (red line) tracks the shape of the statistically predicted amplification (thin black line) for around 12 years, before the curves diverge. The negative projection tracks the statistically predicted amplification for around 25 years[5]. We would not necessarily expect the linear approximations made in the estimation of the leading CSV to hold for the very long lead times, but it is reassuring that, for at least a decade, we find the amplification is well represented by the linear model.

[5]Note that this ensemble was only run for 31 years due to computational constraints.

We are most confident about our amplification estimates for lead times up to $\sim$10 years (Fig. 6). It is of interest to note that these lead times are also when we are most confident that the actual amplification occurs as predicted (Fig. 8). If more ensemble members were used in estimating the CSVs then perhaps the lead times for which we are confident about our amplification estimates could be extended, but this would make the procedure more computationally expensive.

c. Patterns of amplification

It has been shown above that the level of amplification of the largest growing CSV approximately matches the linear prediction for at least 10 years. However, to be confident about using the estimated CSV it is also necessary that the patterns of amplification evolve similarly to that predicted by the linear model. Fig. 9 shows the predicted temperature fields in the subspace of the leading 8 EOFs after 10 years of amplification (top row), and the actual amplification for both the positive (middle row) and negative (bottom row) projections of the leading CSV. Fig. 10 shows the same for the salinity fields.

It is clear from Figs. 9, 10 that the amplified patterns are very similar to those predicted by the linear approximation. Note from that we have scaled the patterns by the appropriate ratios of the estimated amplification factors shown in Fig. 8 for a direct comparison. The largest discrepancies are in the deeper levels, and are slightly larger in salinity than in temperature, but overall these results are encouraging, and give us confidence that our estimates of the CSVs are robust and are working as intended.

d. Amplification mechanism

We now briefly consider how the amplification of anomalies occurs over the first 15 years. Fig. 11a shows the ensemble mean temperature anomaly of the CSV perturbed integrations, averaged over years 8-12. The growth in the North Atlantic Current region is typical of an MOC response in this GCM and a increase in the strength of the sub-polar gyre (e.g. Vellinga and Wu 2004; Dong and Sutton 2005), and as noted in Section 3a, the optimal initial perturbation has a density gradient which is likely to induce an MOC response (Thorpe et al. 2001) through enhanced deep water formation. The timescale of amplification seems to be set by the advective timescales (a few years) in the sub-polar gyre (also see Dong and Sutton 2005), although what processes are setting the timescales of propagation at depth remains an open question, though it is likely a combination of wave and advective processes.

Fig. 11b shows the regression coefficient between ocean temperature and an index of the MOC (defined as the strength of the MOC at 50°N at 1000m depth to consider the higher latitudes where the amplification occurs), but scaled to show the temperature change expected per 0.5Sv increase in the MOC. The patterns closely resemble each other, especially in the deeper levels, suggesting that the change in the MOC is responsible for a significant part of the amplification.

Fig. 12 shows the response of the MOC for the mean of years 8-12 after the perturbation,

for both positive and negative projections. There is a basin wide increase of the MOC (as a response to the positive pattern) in both panels of $0.2 - 0.6$Sv, and this persists for ~ 15 years (not shown). Although the details differ between the positive and negative projections (e.g. the large anomaly in the positive projection near the latitude of the North Atlantic Current), they are broadly consistent in the sign and magnitude of the MOC response. This is possibly due to non-linearities, such as in the deep water formation processes and, although the MOC was in a fairly neutral state at the chosen start date (Fig. 1b), one might expect a lagged response to the previous slight decline of the MOC, which will make the MOC response non-linear to the sign of the perturbation.

It is therefore likely that the MOC response to the perturbed density gradients is the primary driver of the amplification. This finding is in line with previous papers examining MOC variability in this GCM, and with HS09, who also found that an anomalous MOC is responsible for amplification of anomalies in HadCM3. Wider climate impacts of this amplification include a northward shift in the ITCZ and a decrease in Arctic sea ice, consistent with the MOC amplification (not shown).

5. Discussion and conclusions

We have examined the growth of Atlantic Ocean anomalies on decadal timescales in a atmosphere-ocean coupled GCM (HadCM3) to estimate the perturbations which amplify most rapidly. The main findings can be summarised as follows:

- By extending the methods of KTM03 to three dimensions and longer timescales we have demonstrated that initial state dependent climatically relevant singular vectors (CSVs) for use in decadal climate predictions can be reliably estimated for a GCM.

- For the Atlantic domain in HadCM3 the optimal initial regions for growth are found to be the North Atlantic Current region and the main convection sites in the Labrador and Nordic Seas, especially in the top ~ 700m. These regions are therefore identified as being the areas where additional ocean observations would maximally inform decadal climate predictions, for this GCM and particular initial condition.

- An amplification factor of ~ 2 is predicted at a lead time of 15 years. The levels of amplification found in the full non-linear GCM are consistent with that predicted by the linear model for around 15 years, but not on longer lead times.

- Growth of the perturbations mainly occurs in situ, and the mechanism of amplification relies on a perturbation of the Atlantic MOC which initially grows, and then persists for ~ 15 years.

- Although resources have only allowed a single initial condition to be investigated here, the methods used could be streamlined by focussing only on shorter lead times (i.e.

up to 10 years), and hence also reducing the number of ensemble members required. This could reduce the computational resources required by a factor of ~ 8.

We note that our growth estimates have assumed that we can represent the variability with the leading EOFs, but it is possible that a more optimally amplifying mode exists which we cannot capture with this approximation.

In a previous study (HS09) we estimated optimal perturbations for HadCM3 over the same Atlantic domain using a statistical method, namely linear inverse modelling (LIM). The LIM estimates are independent of the specific initial state, and hence represent an average optimal perturbation, whereas the CSV approach has estimated perturbations for a single initial condition. However, the identified regions (the far North Atlantic) are similar in both approaches (and also for a LIM analysis of the GFDL CM2.1 GCM; Tziperman et al. 2008), giving us more confidence in the results. In planned future work we will compare the reliability of the amplification of the LIM and CSV perturbations in both idealised and operational decadal prediction experiments.

Finally, we note that these approaches may help guide development of ocean observing systems for prediction purposes. It is suggested that additional observations in the far North Atlantic would be of most benefit for improving decadal climate predictions, such as those planned for the forthcoming IPCC AR4 (Meehl et al. 2009), although it must be noted that uncertainties in the ocean state below 2000m are greater than near the surface, mainly because of the recent growth in Argo observations, and this has implications for validating predictions also. A future study will examine the robustness of these suggested observation regions across a range of GCMs.

Acknowledgments.

We thank the three anonymous reviewers for their constructive comments which helped improve the paper. The research leading to these results has received funding from the European Community's 7th framework programme (FP7/2007-2013) under grant agreement No. GA212643 (THOR: "Thermohaline Overturning - at Risk", 2008-2012), from the UK Natural Environment Research Council under the thematic Rapid Climate Change programme and from NCAS-Climate. RS was also supported by a Royal Society University Research Fellowship.

REFERENCES

Buizza, R. and T. N. Palmer, 1995: The singular-vector structure of the atmospheric global circulation. *J. Atmos. Sci.*, **52**, 1434–1456.

Collins, M., et al., 2006: Interannual to decadal climate predictability in the North Atlantic: a multimodel-ensemble study. *J. Climate*, **19**, 1195–1202, doi:10.1175/JCLI3654.1.

Czeschel, L., D. P. Marshall, and H. L. Johnson, 2010: Oscillatory sensitivity of Atlantic overturning to high-latitude forcing. *Geophys. Res. Lett.*, **37**, L10 601, doi:10.1029/2010GL043177.

Dong, B. and R. T. Sutton, 2005: Mechanism of interdecadal thermohaline circulation variability in a coupled ocean-atmosphere GCM. *J. Climate*, **18**, 1117 – 1135.

Farrell, B., 1988: Optimal excitation of neutral Rossby waves. *J. Atmos. Sci.*, **45**, 163 – 172.

Farrell, B. and P. J. Ioannou, 2001: Accurate low-dimensional approximation of the linear dynamics of fluid flow. *J. Atmos. Sci.*, **58**, 2771–2789.

Gardiner, C. W., 1985: *Handbook of Stochastic Methods for Physics, Chemistry, and the Natural Sciences*. Springer, 442 pp.

Gordon, C., C. Cooper, C. A. Senior, H. Banks, J. M. Gregory, T. C. Johns, J. F. B. Mitchell, and R. A. Wood, 2000: The simulation of SST, sea ice extents and ocean heat transports in a version of the Hadley Centre coupled model without flux adjustments. *Climate Dyn.*, **16**, 147–168.

Griffies, S. M. and K. Bryan, 1997: Predictability of North Atlantic multidecadal climate variability. *Science*, **275**, 181–184.

Grist, J. P., S. A. Josey, and B. Sinha, 2007: Impact on the ocean of extreme Greenland Sea heat loss in the HadCM3 coupled ocean-atmosphere model. *J. Geophys. Res.*, **112**, C04014, doi:10.1029/2006JC003629.

Hawkins, E., J. Robson, R. Sutton, D. Smith, and N. Keenlyside, 2010: Evaluating the potential for statistical decadal predictions of sea surface temperatures with a perfect model approach. *Clim. Dyn.*, submitted.

Hawkins, E. and R. Sutton, 2007: Variability of the Atlantic thermohaline circulation described by three-dimensional empirical orthogonal functions. *Climate Dyn.*, **29**, 745–762, doi:10.1007/s00382-007-0263-8.

Hawkins, E. and R. Sutton, 2009a: Decadal predictability of the Atlantic Ocean in a coupled GCM: estimation of optimal perturbations using Linear Inverse Modelling. *J. Climate*, **22**, 3960–3978, doi:10.1175/2009JCLI2720.1.

Hawkins, E. and R. Sutton, 2009b: The potential to narrow uncertainty in regional climate predictions. *Bull. Amer. Met. Soc.*, **90**, 1095–1107, doi:10.1175/2009BAMS2607.1.

Keenlyside, N. S., M. Latif, J. Jungclaus, L. Kornblueh, and E. Roeckner, 2008: Advancing decadal-scale climate prediction in the North Atlantic sector. *Nature*, **453**, 84–88, doi: 10.1038/nature06921.

Kleeman, R., Y. Tang, and A. M. Moore, 2003: The calculation of climatically relevant singular vectors in the presence of weather noise as applied to the ENSO problem. *J. Atmos. Sci.*, **60**, 2856 – 2868.

Meehl, G. A., et al., 2007: *Global climate projections. In: Climate Change 2007: The Physical Science Basis. Contribution of Working Group I to the Fourth Assessment Report of the Intergovernmental Panel on Climate Change*. Cambridge University Press, Cambridge, UK.

Meehl, G. A., et al., 2009: Decadal prediction: can it be skillful? *Bull. Amer. Met. Soc.*, **90**, 1467–1485, doi:10.1175/2009BAMS2607.1.

Molteni, F., R. Buizza, T. N. Palmer, and T. Petroliagis, 1996: The ECMWF Ensemble Prediction System: methodology and validation. *Q. J. Royal Met. Soc.*, **122**, 73–119, doi:10.1002/qj.49712252905.

Moore, A. M. and R. Kleeman, 2001: The differences between the optimal perturbations of coupled models of ENSO. *J. Climate*, **14**, 138–163.

Palmer, T. N., 1993: Extended-range atmospheric prediction and the Lorenz attractor. *Bull. Amer. Met. Soc*, **74**, 49–65.

Palmer, T. N., R. Gelaro, J. Barkmeijer, and R. Buizza, 1998: Singular vectors, metrics, and adaptive observations. *J. Atmos. Sci.*, **55**, 633–653.

Pardaens, A. K., H. T. Banks, J. M. Gregory, and P. R. Rowntree, 2003: Freshwater transports in HadCM3. *Climate Dyn.*, **21**, 177–195, doi:10.1007/s0038200303246.

Penland, C. and P. D. Sardeshmukh, 1995: The optimal growth of tropical sea surface temperature anomalies. *J. Climate*, **8**, 1999 – 2024.

Pohlmann, H., M. Botzet, M. Latif, A. Roesch, M. Wild, and P. Tschuck, 2004: Estimating the decadal predictability of a coupled AOGCM. *J. Climate*, **17**, 4463–4472.

Pohlmann, H., J. Jungclaus, A. Kohl, D. Stammer, and J. Marotzke, 2009: Initializing decadal climate predictions with the GECCO oceanic synthesis: Effects on the North Atlantic. *J. Climate*, **22**, 3926–3938, doi:10.1175/2009JCLI2535.1.

Sevellec, F., T. Huck, M. B. Jelloul, N. Grima, J. Vialard, and A. Weaver, 2008: Optimal surface salinity perturbations of the meridional overturning and heat transport in a global ocean general circulation model. *J. Phys. Ocean.*, **38**, 2739–2754.

Sevellec, F., M. B. Jelloul, and T. Huck, 2007: Optimal surface salinity perturbations influencing the thermohaline circulation. *J. Phys. Ocean.*, **37**, 2789–2808.

Smith, D. M., S. Cusack, A. W. Colman, C. K. Folland, G. R. Harris, and J. M. Murphy, 2007: Improved surface temperature prediction for the coming decade from a global climate model. *Science*, **317**, 796–799, doi:10.1126/science.1139540.

Thorpe, R. B., J. M. Gregory, T. C. Johns, R. A. Wood, and J. F. B. Mitchell, 2001: Mechanisms determining the Atlantic thermohaline circulation response to greenhouse gas forcing in a non-flux-adjusted coupled climate model. *J. Climate*, **14**, 3102–3116.

Toth, Z. and E. Kalnay, 1997: Ensemble forecasting at NCEP and the breeding method. *Mon. Weather Rev.*, **125**, 3297 – 3319.

Tziperman, E., L. Zanna, and C. Penland, 2008: Non-normal thermohaline circulation dynamics in a coupled ocean-atmosphere GCM. *J. Phys. Ocean.*, **38**, 588 – 604, doi: 10.1175/2007JPO3769.1.

Vellinga, M. and P. Wu, 2004: Low-latitude freshwater influence on centennial variability of the Atlantic thermohaline circulation. *J. Climate*, **17**, 4498–4511.

Zanna, L., P. Heimbach, A. M. Moore, and E. Tziperman, 2010: Optimal excitation of interannual Atlantic meridional overturning circulation variability. *J. Climate*, in press.

Zanna, L. and E. Tziperman, 2005: Non-normal amplification of the thermohaline circulation. *J. Phys. Ocean*, **35**, 1593–1605.

List of Figures

(a)

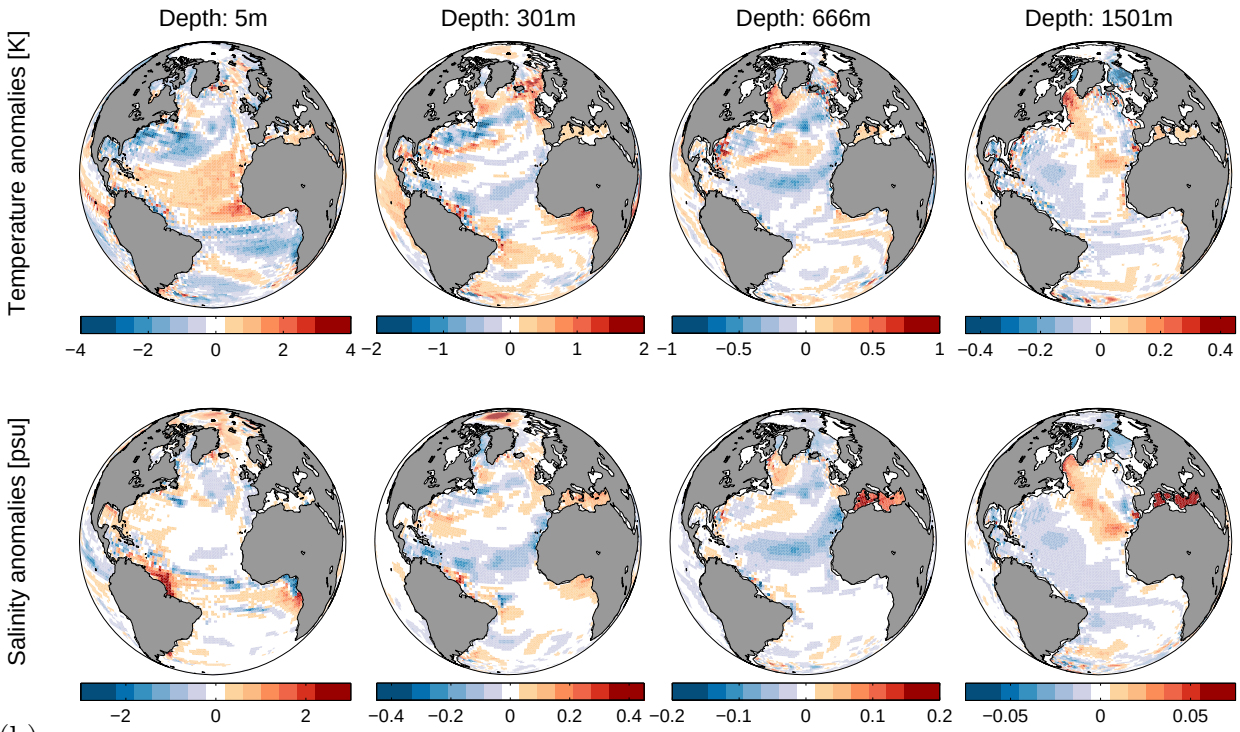

(b)

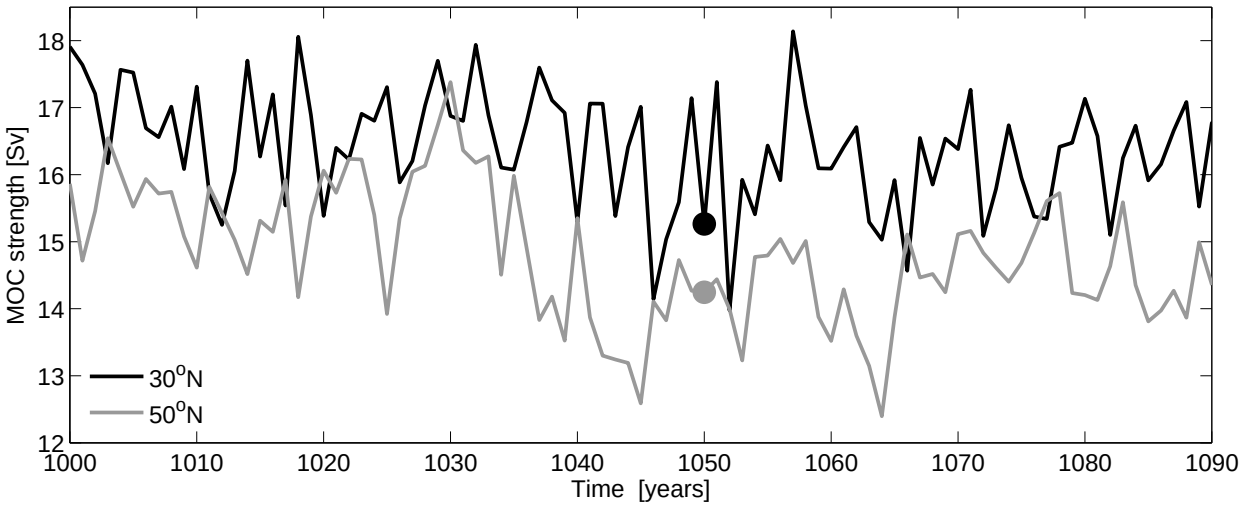

FIG. 1. (a) The instantaneous initial condition anomalies from the time mean of the control run, at depths as labelled. Top row: temperature (K). Bottom row: salinity (psu). (b) The meridional overturning circulation at 1000m depth at 30°N (MOI, black) and 50°N (grey), with the starting year shown as the solid points. The panel shows a 90 year segment of the 1100 year control run. The long term mean of the MOC at 30°N (50°N) is 16.3Sv (14.8 Sv).

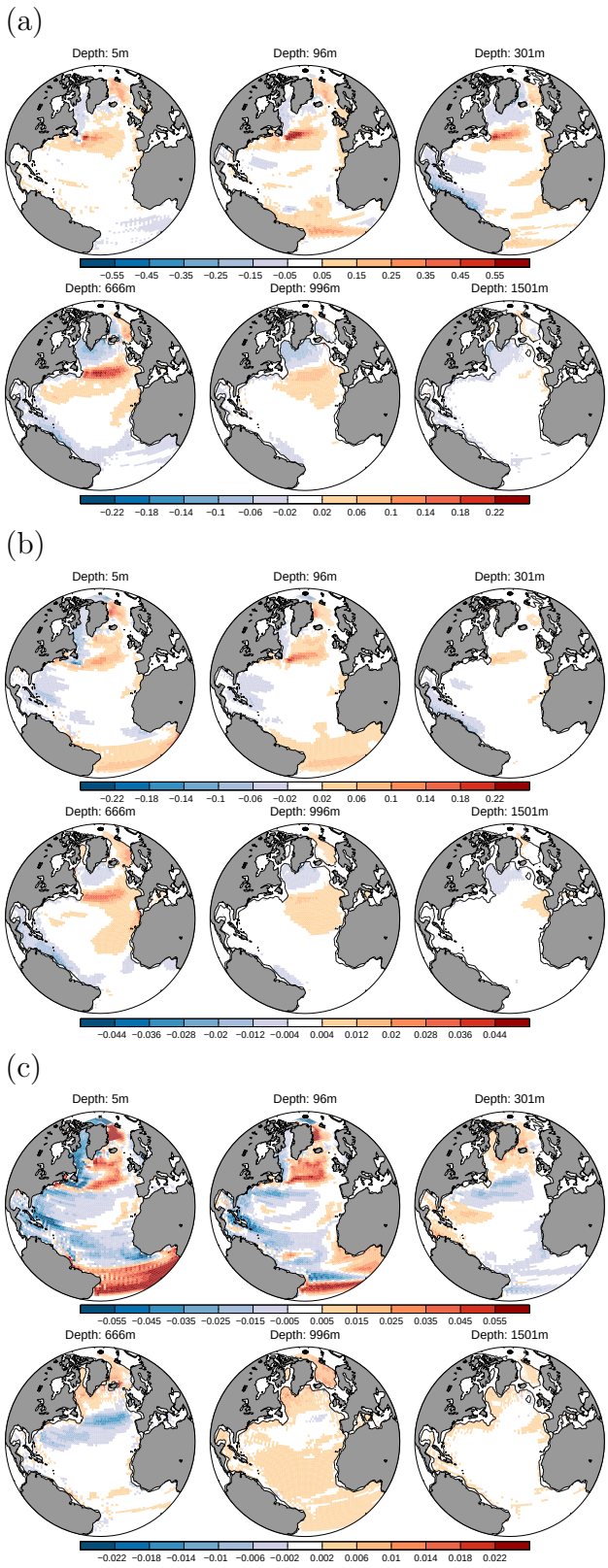

FIG. 2. The optimal initial condition of the leading CSV, optimised for maximal amplification at a lead time of 10 years, on depth levels as labelled. (a) Temperature in K. (b) Salinity in psu. (c) Density in kg m^{-3}. Note the different colour scales for the deeper levels.

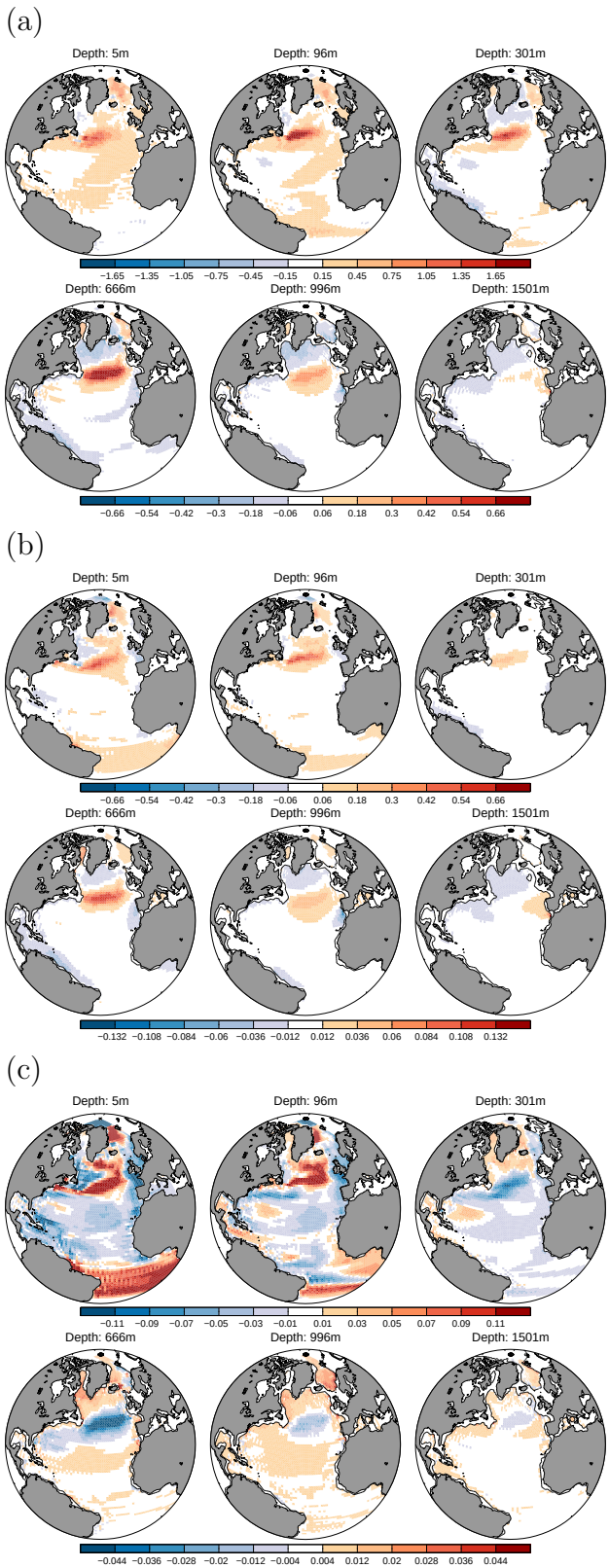

FIG. 3. The maximally amplified pattern of the leading CSV, optimised for maximal amplification at a lead time of 10 years, on depth levels as labelled. (a) Temperature in K. (b) Salinity in psu. (c) Density in kg m^{-3}. Note that the colour scales are different from Fig. 2.

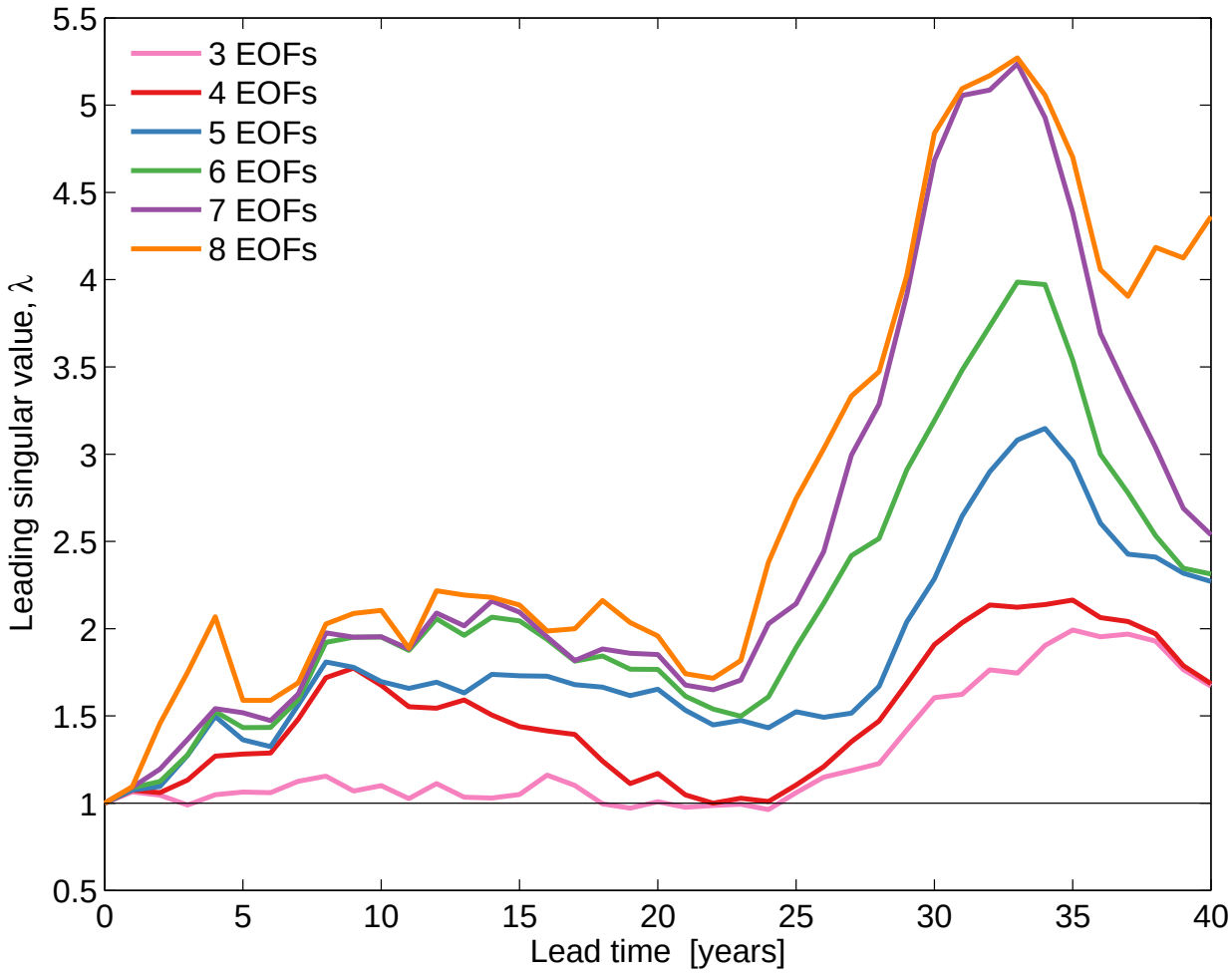

FIG. 4. Maximum amplification curves using various numbers of EOFs (M) as labelled. The amplification seems to be converging with 8 EOFs.

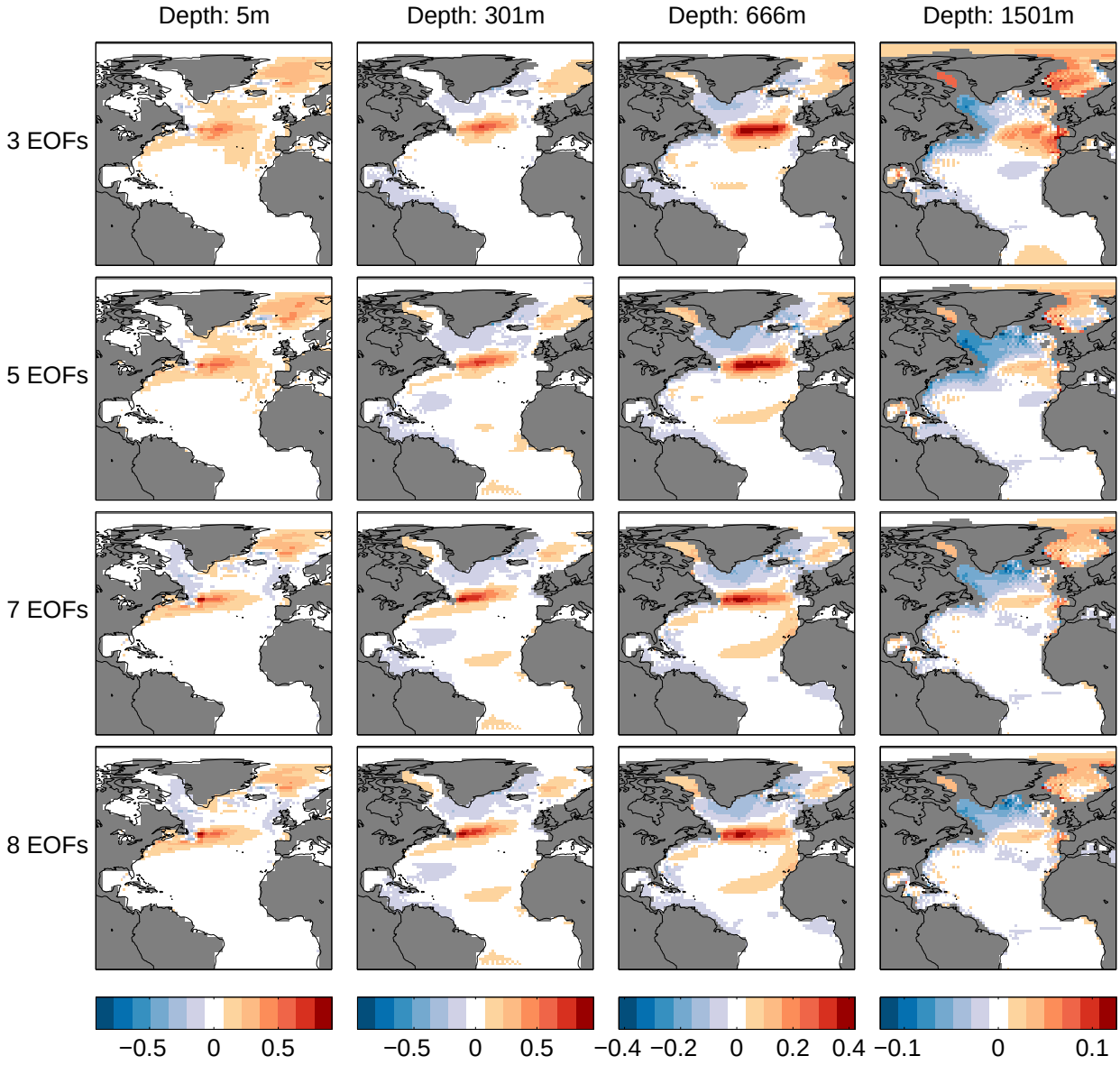

FIG. 5. The convergence of the leading initial CSV pattern for temperature, with number of EOFs used, optimised for a lead time of 33 years, plotted on depth levels as indicated.

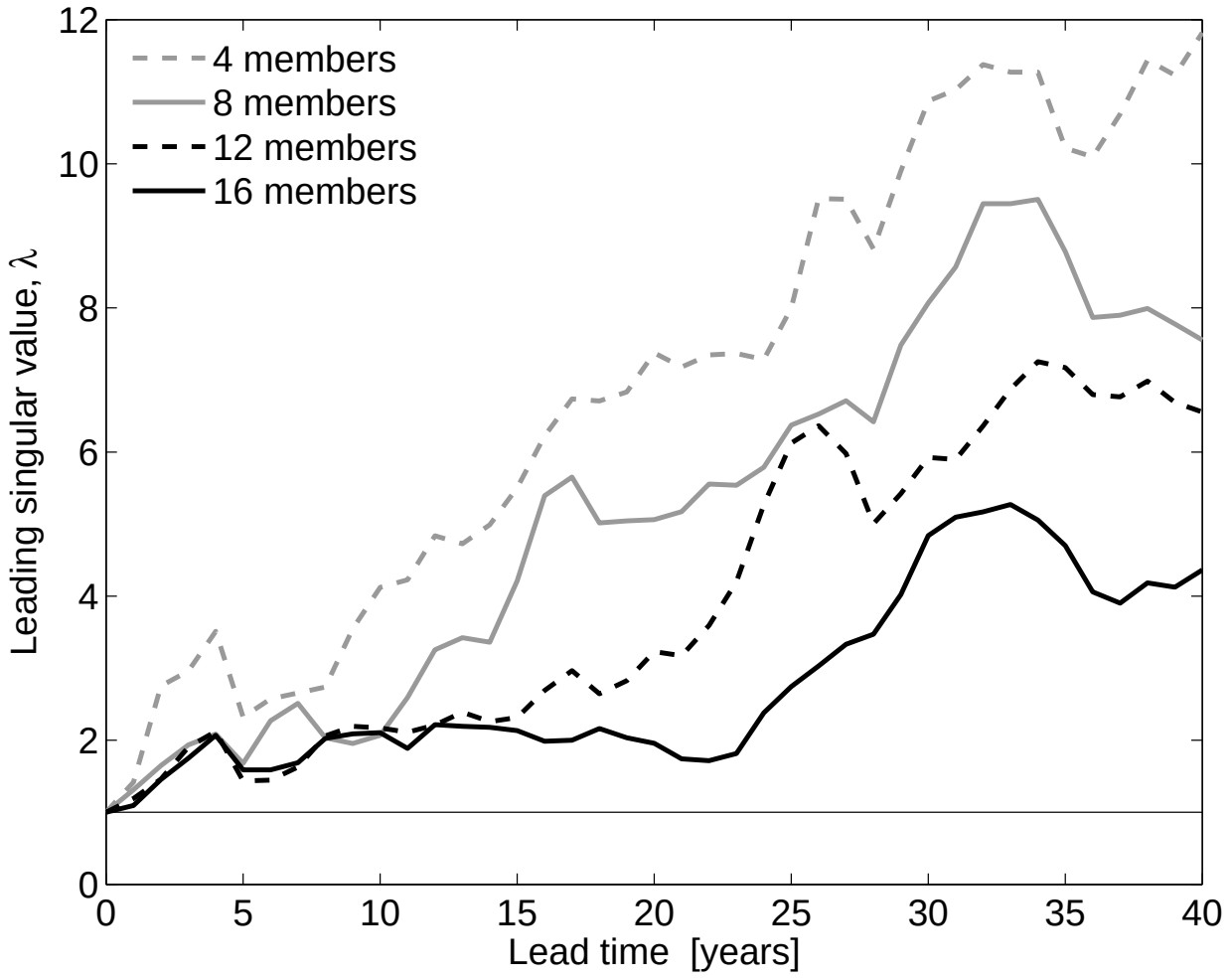

FIG. 6. Maximum amplification curves, using 8 EOFs, for various numbers of ensemble members (K) as labelled. There is convergence in the amplification estimates for lead times up to around 10 years, but not beyond.

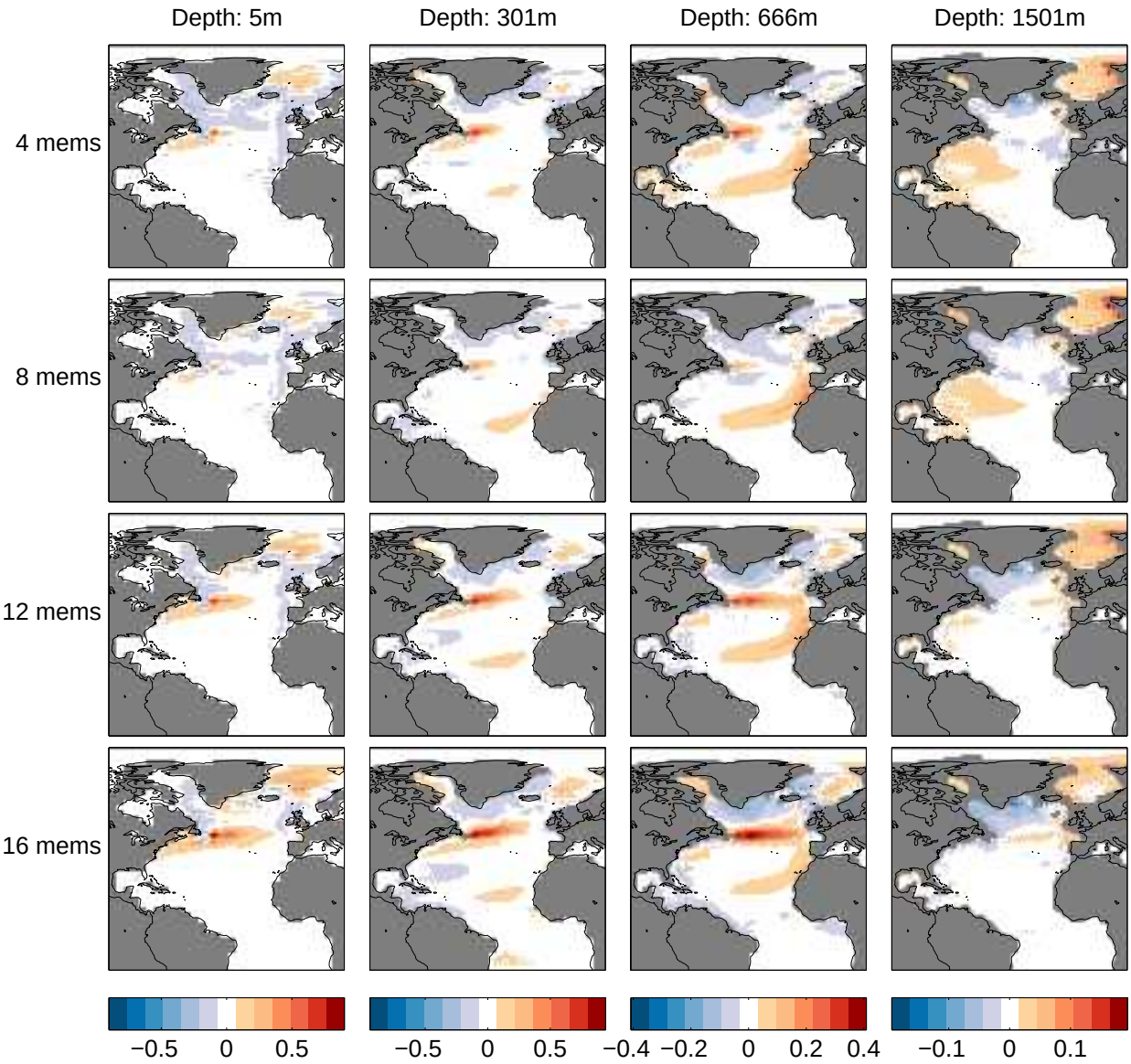

FIG. 7. The convergence of the leading initial CSV pattern for temperature, with number of ensemble members, optimised for a lead time of 33 years, plotted on depth levels as indicated.

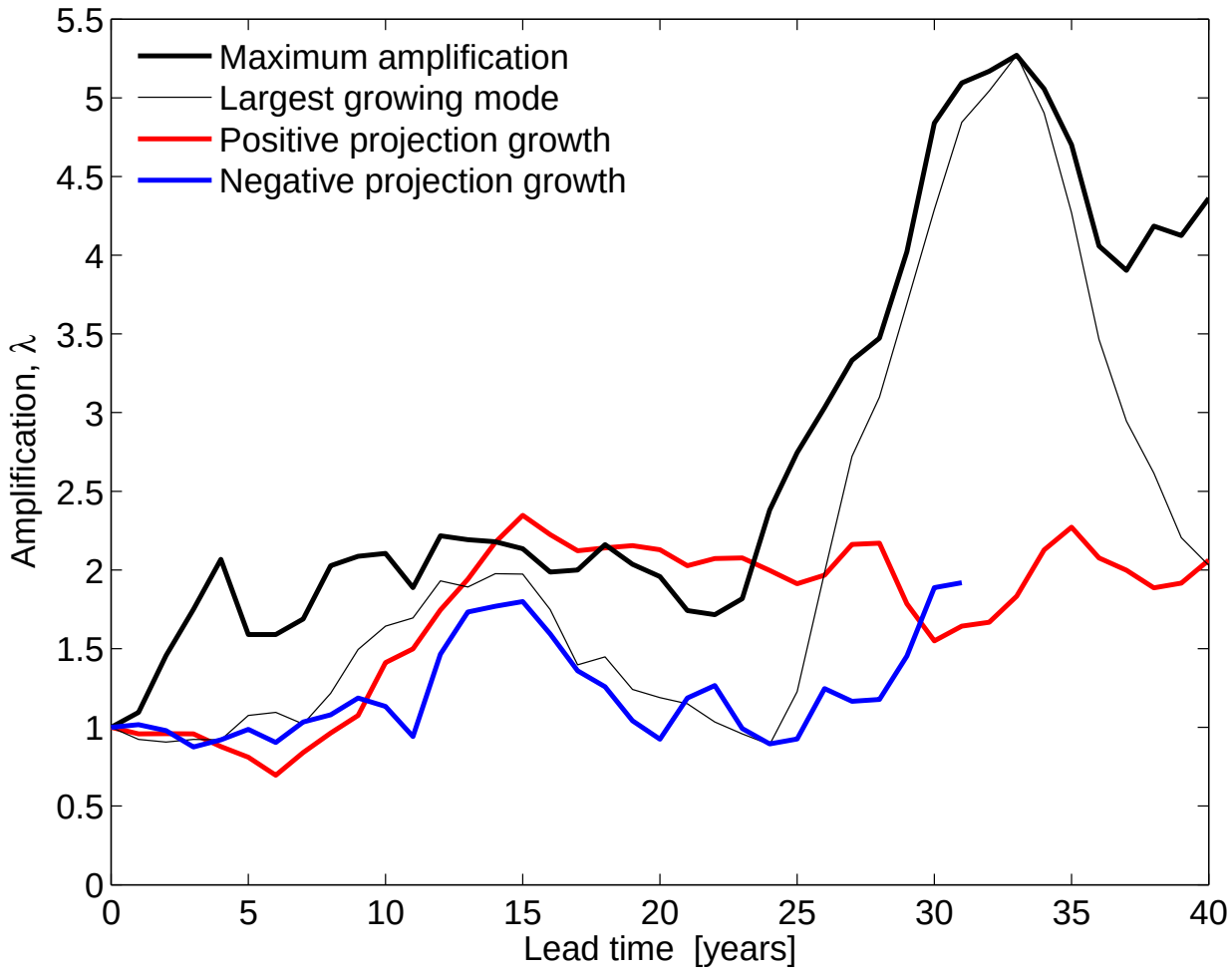

FIG. 8. The maximum amplification curve (thick black line), predicted amplification of the leading CSV for a 33 years optimisation time (thin black line) and the actual amplification of the leading CSV with positive projection (red line) and negative projection (blue line).

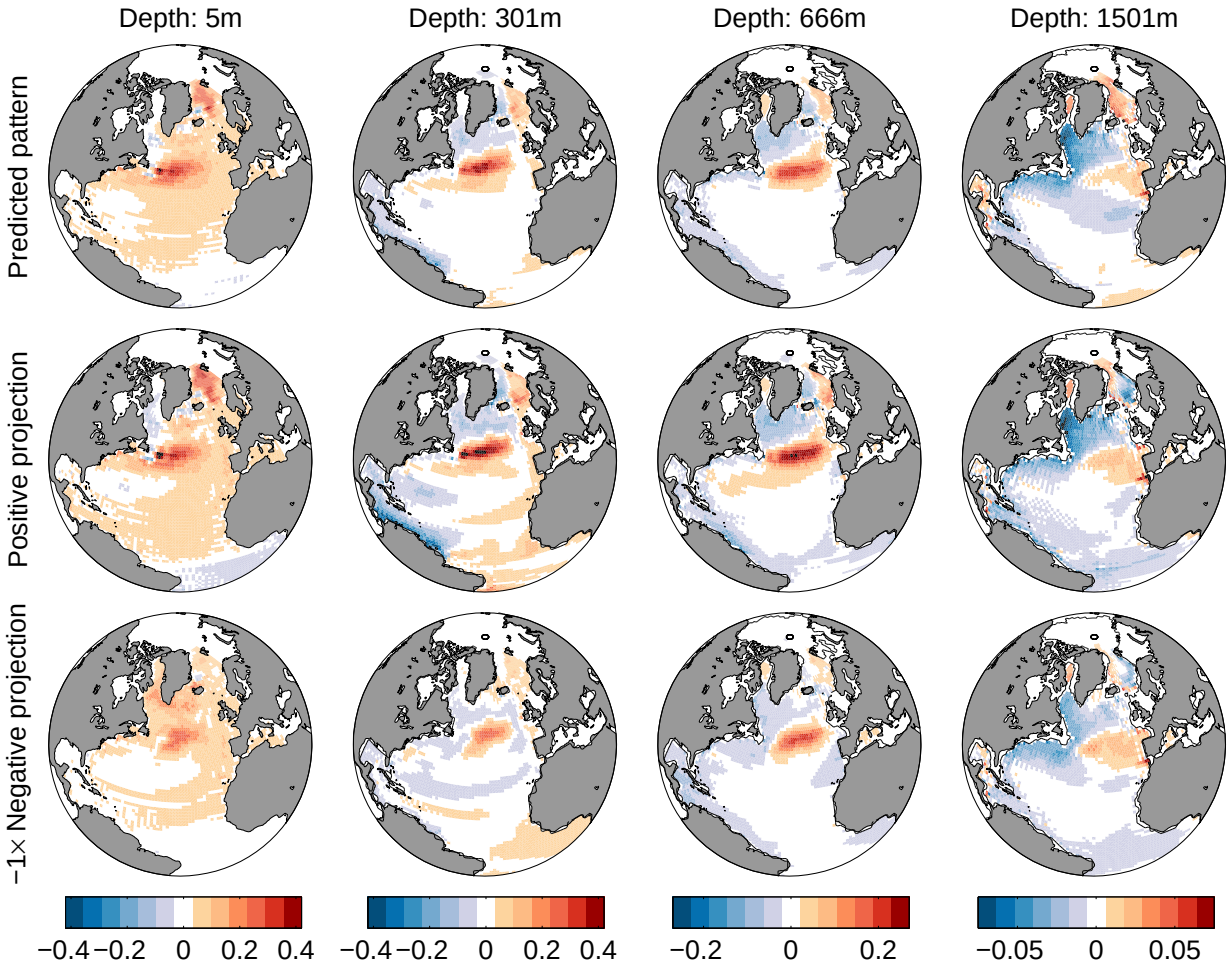

FIG. 9. Comparing the patterns of amplification for temperature (in K) after 10 years, in the subspace of the leading 8 EOFs. Top row: predicted pattern. Middle row: Actual amplification for a positive projection of the leading CSV. Bottom row: Actual amplification for a negative projection of the leading CSV.

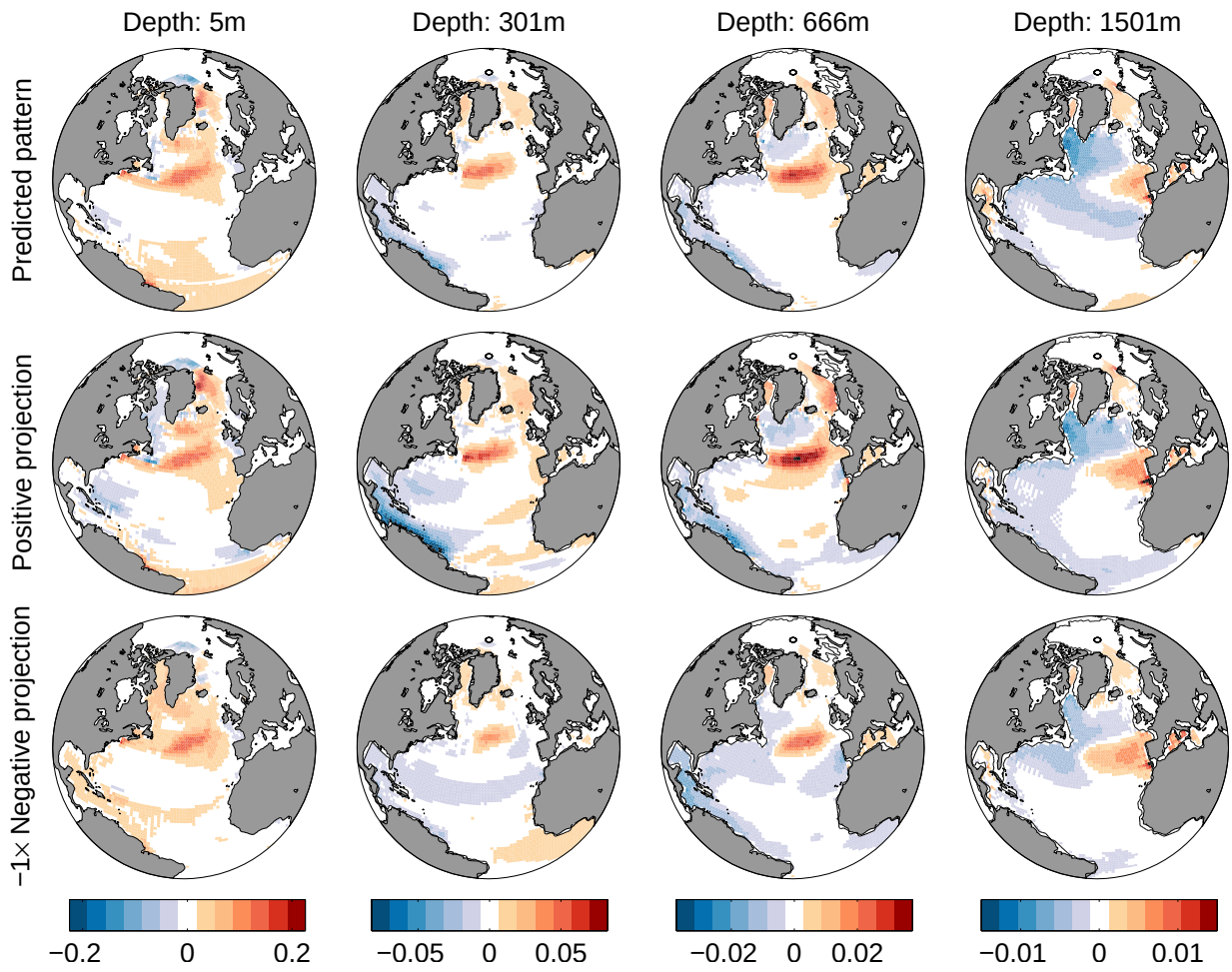

FIG. 10. Same as Fig. 9 for salinity, in psu.

(a)

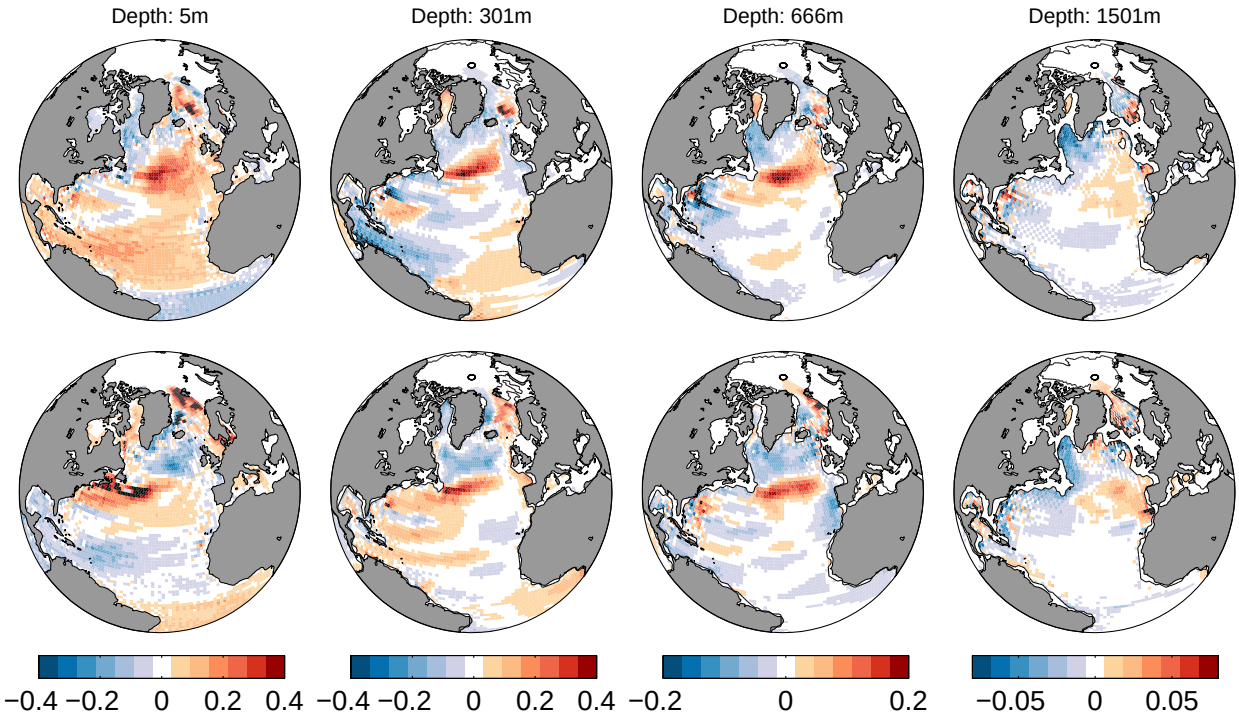

(b)

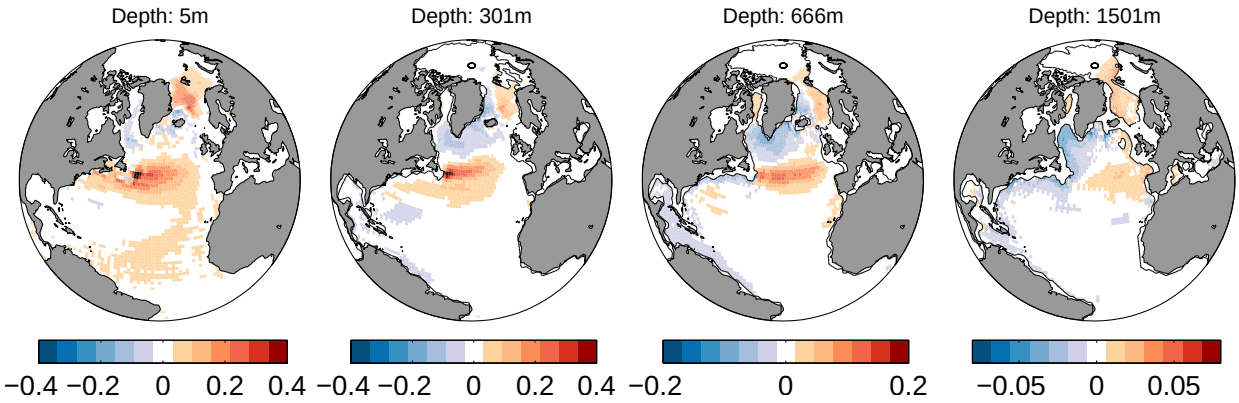

FIG. 11. (a) The temperature anomaly (in K), of the positive (top) and $-1\times$ negative (bottom) CSV perturbed integration, averaged between years 8-12. (b) Regression between the meridional overturning index at 50°N and ocean temperature, in K/0.5Sv, on depth levels as labelled.

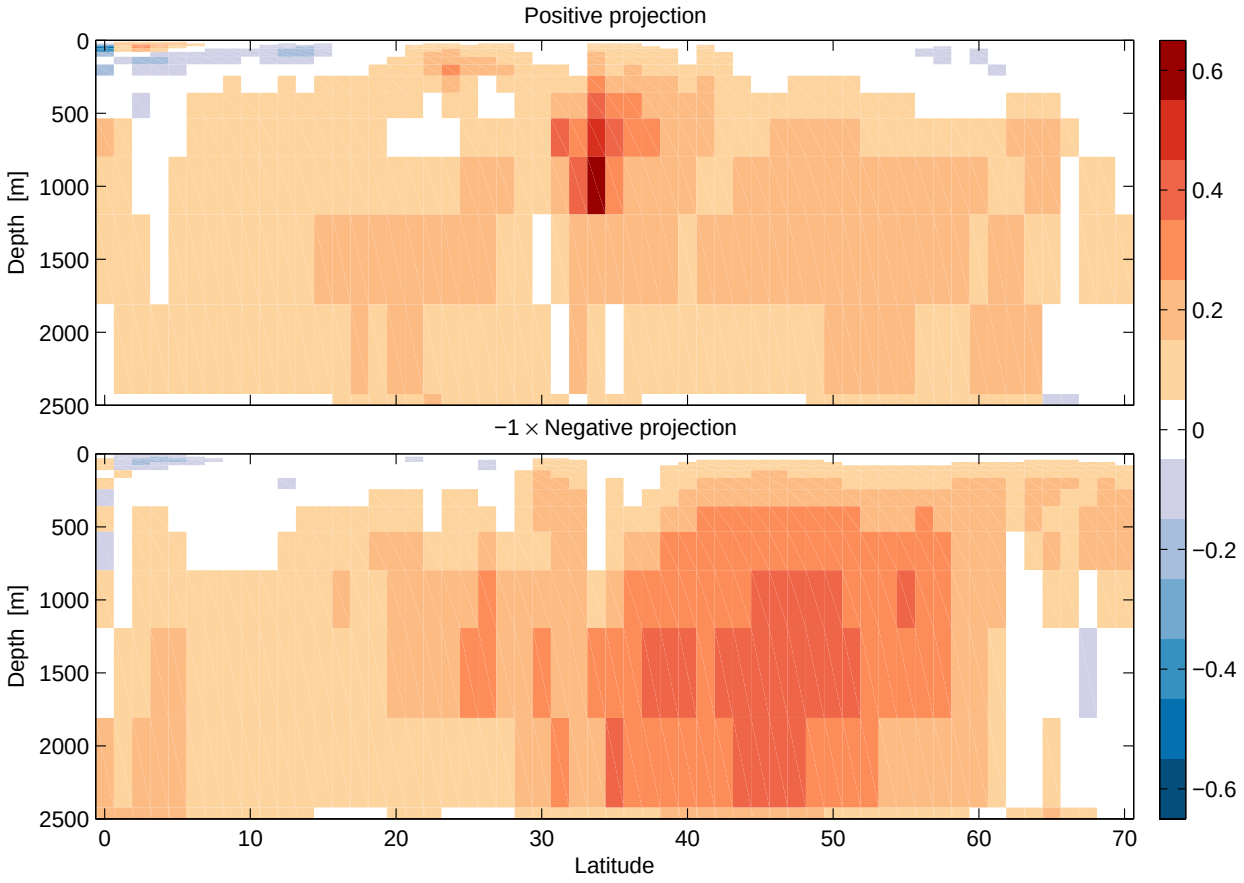

FIG. 12. The response of the MOC (in Sv) to the optimal perturbation, averaged over years 8-12. Top panel: using the positive projection. Bottom panel: using the negative projection.